International Journal of Research in Engineering and Science (IJRES)
ISSN (Online): 2320-9364, ISSN (Print): 2320-9356
www.ijres.org Volume 13 Issue 1 ǁ January 2025 ǁ PP. 147-156

Simulation of storm-induced waves in the East Sea (Vietnam) using combined data from global reanalysis wind datasets and empirical models

Nguyen Xuan Hien*, Duong Ngoc Tien, Nguyen Thanh Trang, Cao Hoang Anh, Vu Thi Vui, Pham Van Chinh
Center for Oceanography, Viet Nam Meteorological and Hydrological Administration

Abstract: *This study investigates the simulation of storm-induced waves using global reanalysis wind data from the European Centre for Medium-Range Weather Forecasts (ECMWF) in conjunction with the empirical storm wind model developed by Boose et al., serving as the storm-influenced wind field. The MIKE 21 SW model was applied to simulate wave dynamics in the East Sea (Vietnam), Vietnam, for selected storms between 2016 and 2021. Validation against wave height observations from the Jason-3 satellite demonstrated that the integration of the combined wind data notably improved statistical performance metrics, including the Pearson correlation coefficient (r), Root Mean Square Error (RMSE), and Nash-Sutcliffe Efficiency (NSE), when compared to simulations using reanalysis wind data alone. Furthermore, the combined wind dataset yielded wave height simulations that closely aligned with satellite observations in storm-affected regions, underscoring its utility in enhancing storm wave modeling for Vietnam's coastal areas.*

Keywords: *Storm waves; Extreme waves; Global reanalysis wind; MIKE 21 SW; East Sea (Vietnam)*

Date of Submission: 17-01-2025 Date of acceptance: 31-01-2025

I. Introduction

Wave data is a critical foundation in oceanographic research and various practical applications. Accurate information on ocean waves supports the forecasting and warning of marine disasters, the design of maritime infrastructure, maritime safety, and socio-economic development activities. However, direct wave measurements from observation stations, drifting buoys, ships, radars, or satellites are often limited in spatial and temporal coverage. To address these gaps, numerical wave models have emerged and developed significantly over the past few decades, providing an effective tool for wave simulations [1–7]. Advanced wave spectral theories and third-generation wave models, such as WAM, WAVEWATCH-III, SWAN, and MIKE 21 SW, have enabled studies of wind-wave regimes on larger spatial and temporal scales.

Despite their advantages, global numerical models using reanalysis wave data often fail to accurately capture extreme wave conditions under severe weather events such as storms, tropical cyclones, or oceanic whirlpools. Consequently, these models tend to underestimate wave heights during such events [8, 9]. To improve storm wave simulations, various wind data sources have been explored in previous studies. One approach involves using experimental storm wind models to construct wind fields [10-13]. These models are straightforward to implement and effectively calibrate waves in storm-affected areas. However, their reliability diminishes in regions far from the storm center, where the spatial distribution of simulated waves often deviates significantly from reality [14]. Another approach uses wind fields derived from global meteorological models and regional-scale dynamic weather models. This method provides detailed spatial and temporal simulations, producing wave distributions that align more closely with observations [15-16]. However, these models require significant computational resources and processing time to recreate meteorological fields [1].

Recently, reanalysis of wind datasets, such as those provided by NOAA and ERA5, have been widely applied in storm wave simulations [17]. These datasets are user-friendly and generally yield wave simulation results with realistic spatial and temporal distributions. Nonetheless, in storm-affected areas, they often underestimate wave heights compared to actual observations [18-21]. To address these limitations, a combined approach has gained traction. This method integrates wind data from dynamic meteorological models and semi-empirical techniques, leveraging the strengths of both while minimizing their respective weaknesses [22-24].

In this study, a combined approach is applied to simulate storm-induced waves in the East Sea (Vietnam). The global reanalysis wind data from the European Centre for Medium-Range Weather Forecasts (ECMWF) are used as the background wind field, combined with the experimental storm wind model developed by Boose et al. (1994) [25] for storm-affected regions. The MIKE 21 SW model is employed to simulate storm waves for representative events between 2016 and 2021. Observational wave data from the Jason-3 satellite are used to

evaluate the effectiveness of this combined wind data approach in improving storm wave simulations for Vietnam's coastal waters.

II. Research methods and data

2.1. Research data

The wave and global reanalysis wind data from the East Sea (Vietnam) include 10-meter level wind parameters (wind direction and speed) as well as wave characteristics (significant wave height, mean wave direction, and mean wave period). These datasets were obtained from the European Centre for Medium-Range Weather Forecasts (ECMWF) [26]. The data cover the period from 1979 to 2022, with a temporal resolution of 1 hour. The spatial domain is defined by the coordinates (99.0°E–121.0°E; 0.0°N–23.0°N), with a spatial resolution of 0.25° × 0.25° in latitude and longitude. The historical storm dataset, obtained from the Digital Storm platform of the National Institute of Informatics (NII), Japan [27], encompasses information on wind speed, maximum wind radius, and central pressure of storms. All data are provided in NetCDF format.

The seabed topography data of the East Sea (Vietnam), at a scale of 1:50,000, was supplied by the Vietnam Administration of Seas and Islands as part of the project titled "Determination of the Mean Tide Level and the Lowest Mean Sea Level Line of Vietnam's Maritime Area for State Management of Seas and Islands." Additionally, topographic data for adjacent maritime regions was obtained from the National Geophysical Data Center (NGDC) of the United States.

The wave data utilized in this study was collected by the Jason-3 satellite. Jason-3 continues the legacy of the Topex/Poseidon, Jason-1, and Jason-2 missions, extending the global record of high-precision ocean altimetry essential for climate monitoring, operational oceanography, and seasonal forecasting. This mission, developed through a collaborative partnership involving CNES, NASA, EUMETSAT, and NOAA, builds on over two decades of sustained oceanographic observations. In this partnership, NOAA and EUMETSAT assume leadership of mission operations, with CNES coordinating system management and NASA contributing to the scientific and operational efforts. As a critical component of the satellite altimetry constellation, Jason-3 incorporates significant advancements in both system architecture and data processing, ensuring improved performance over its predecessor, Jason-2. The satellite is constructed on the Proteus platform and is equipped with advanced altimetry instrumentation designed to deliver precise ocean surface height measurements. Jason-3 maintains the traditional T/P-Jason orbit, characterized by a non-sun-synchronous configuration at an altitude of 1,336 km and an inclination of 66°. Between its launch and April 7, 2022, Jason-3 operated in its designated nominal orbit. On April 25, 2022 (Cycle 300), the satellite transitioned to an interleaved orbit previously employed by Topex (2002–2005), Jason-1 (2009–2012), and Jason-2 (October 2016–July 2017). This transition ensures continuity in the long-term oceanographic data record, reinforcing Jason-3's role in supporting the scientific and operational needs of the global oceanographic community.

Based on wave data obtained from satellite observations and the collected storm tracks, the study selected storms whose wave tracks, as observed by satellite, passed through areas directly affected by the storm. The list of selected storms is presented in Table 1.

Table 1. Information of selected storm

No.	Storm name	Start time	End time	Satellite	Satellite Track Time
1	Sarika (2016)	2016-10-12 18:00:00	2016-10-20 06:00:00	Jason-3	2016-10-16 20:00:00
2	Tokage (2016)	2016-11-23 06:00:00	2016-11-28 00:00:00	Jason-2	2016-11-26 11:00:00
3	Mawar (2017)	2017-08-30 06:00:00	2017-09-04 06:00:00	Jason-3	2017-09-03 15:00:00
4	Ewiniar (2018)	2018-06-02 06:00:00	2018-06-11 06:00:00	Jason-3	2018-06-05 07:00:00
5	Pabuk (2019)	2018-12-30 12:00:00	2019-01-07 18:00:00	Jason-3	2019-01-07 23:00:00
6	Etau (2020)	2020-11-08 12:00:00	2020-11-10 18:00:00	Jason-3	2020-11-08 04:00:00
7	Lionrock (2021)	2021-10-02 18:00:00	2021-10-10 18:00:00	Jason-3	2021-10-08 08:00:00

2.2. Research methods

2.2.1. Wave simulation model

The MIKE 21 SW model was selected for simulating storm wave dynamics. It is a module within the MIKE software suite, developed by the Danish Hydraulic Institute (DHI). MIKE 21 SW is specifically designed to simulate the generation, attenuation, and propagation of wind-generated waves and swell waves in both deep and shallow water environments. Its primary objective is to predict and evaluate wave dynamics in offshore and coastal regions. The model accounts for key processes such as wave refraction, shallow water effects, wind influences, energy dissipation due to bottom friction, wave breaking, and wave-current interactions. Additionally, MIKE 21 SW incorporates wave diffraction through the solution of the mild-slope wave equation.

2.2.2. Experimental storm wind model

The storm wind model proposed by Bose et al. (1994) [25] is employed to simulate and calculate the wind field distribution during a storm. The model determines the wind field at specific time intervals for locations both within and beyond the storm's eye. Key input parameters for the wind field calculation include the storm center's coordinates, the storm's trajectory and speed, the radius of the storm's eye, the maximum wind speed, and surface characteristics.

The formula for calculating the wind velocity at a point *S(x,y)* located within the eye of the storm is expressed as:

$$V_s = F[V_m - V_f(1-\sin\theta)]\frac{R}{R_{mw}} \quad (1)$$

The formula for calculating the wind velocity at a point *S(x,y)* located outside the eye of the storm is given by:

$$V_s = F[V_m - V_f(1-\sin\theta)](\frac{R_{mw}}{R})^x \quad (2)$$

Where: F is the wind reduction coefficient due to terrain (land: 0.8, sea: 1.0); V_m is the maximum wind speed over the sea (*m/s*); V_f is the storm's movement speed (*m/s*); θ is the clockwise angle of the straight line connecting point *S(x,y)* with the storm center (π) and the storm's direction of movement; R is the distance from point *S(x,y)* to the storm center (*km*); R_{mw} is the storm's maximum wind radius (*km*); x is the wind profile coefficient for each storm (according to Simpson and Riehl, 1981, $0.4 < x < 0.8$).

2.2.3. Combination of the experimental storm wind model and reanalysis wind

Within the region influenced by the storm's maximum wind radius, the storm wind field model proposed by Bose et al. (1991) is utilized. For locations situated beyond twice the maximum wind radius (R_{mw}) from the storm center, the reanalysis wind data from the European Centre for Medium-Range Weather Forecasts (ECMWF) is applied as the background wind field. In the transition area between R_{mw} and 2 R_{mw}, the storm wind is calculated based on a distance-weighted method, as follows:

$$V = V_s \text{ (with } r \le R_{mw}) \quad (3)$$

$$V = (1 - \alpha)\, V_s + \alpha\, V_{re} \text{ (with } R_{mw} < r < 2R_{mw}) \quad (4)$$

$$V = V_{re} \text{ (with } r \ge 2R_{mw}) \quad (5)$$

Where, V is the storm wind speed at any given point; V_s is the experimental wind speed calculated from formulas 1 and 2; V_{re} is the reanalysis wind speed; r is the distance from the wind speed calculation point to the storm center; α is the distance-weighted conversion coefficient, $\alpha = (r - R_{mw}) / R_{mw}$.

2.3. Model setup

The data sources for the coastline and topography utilized in constructing the computational grid for scenarios involving reanalysis wind and storm wind simulations are as follows:

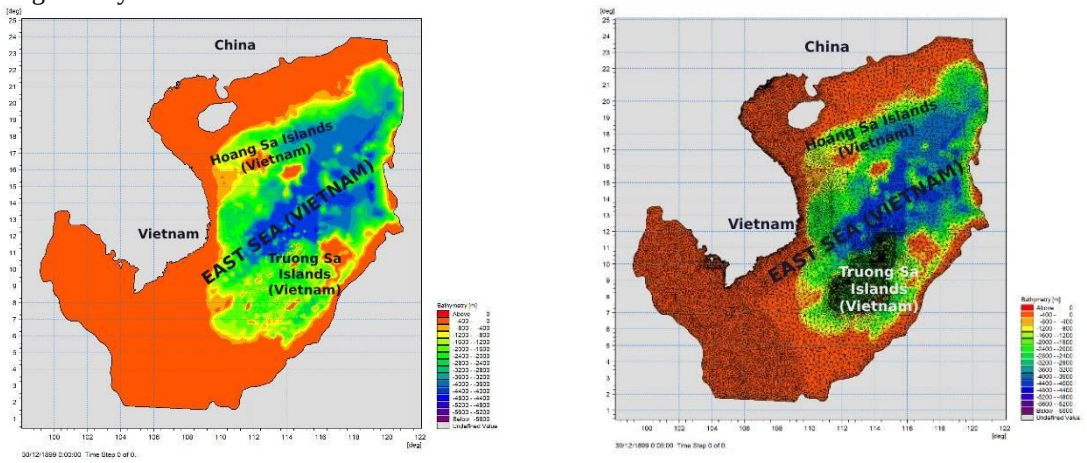

Figure 1. Seabed topography (left) and computational grid (right) of the East Sea (Vietnam)

The computational grid of the East Sea (Vietnam) is employed to simulate the wave field under storm conditions for both scenarios. The grid is designed with coarser mesh spacing in offshore areas, gradually transitioning to finer resolution near the coastline and around the Spratly Islands. The detailed grid parameters are presented in Table 2.

Table 2. Grid parameters

Parameters	East Sea (Vietnam) Computational Grid
Coordinate system	LON/LAT
Number of nodes	16,570
Number of triangles	31,845
Number of loose boundary points	8
Highest resolution	200m
Lowest resolution	25,000m

The initial conditions are defined using the experimental spectrum formula of JONSWAP. At the sea boundary, wave parameters such as height, direction, and period are derived from reanalysis wave data. For the surface boundary conditions, reanalysis wind field data is used for Scenario 1, while wind field data incorporating storm swirl is applied for scenario 2. Rigid boundary conditions are enforced with impermeable constraints at the boundary limits.

Basic parameters for the wave model: Time step: 60s for the East Sea (Vietnam) grid; Apply the full spectrum formula; Fourth-order wave interaction; Two wave dissipation coefficients: Cdis = 4.5, DELTA = 0.5; Seabed roughness coefficient: Nikuradse parameter Kn = 0.04 applied uniformly across the model area; Energy dissipation ratio: $\alpha = 1$; Wave breaking condition: $\gamma = Hs/h = 0.8$ (Hs - wave height, h - water depth).

2.4. Model calibration and validation

2.4.1. Data sources for calibration and validation

The input parameters of the storms used in the study, the Sarika storm (2016) for calibration and the Doksuri storm (2017) for model validation, were collected from the Digital Storm website of the National Institute of Informatics (NII).

2.4.2. Evaluation criteria

This study uses three evaluation criteria, including: Pearson correlation coefficient (r), root mean square error (RMSE) ratio (RSR), and Nash-Sutcliffe efficiency coefficient (NSE). The quality assessment criteria for the calculation results based on these three indicators are shown in Table 3 [28].

The Pearson correlation coefficient (r) is calculated as follows:

$$r = \frac{\mathrm{cov}(x, y)}{\sigma_x . \sigma_y} \tag{6}$$

Where, the observed data (x) and model data (y); cov(x, y) is the covariance between the two variables x and y, and the value ranges from -1 to 1. The coefficient r is an important measure to assess the similarity between the two data series, with r closer to 1 indicating higher similarity between the two series, and vice versa.

Table 3. Standards for assessing the quality of calculated data based on three indicators

Quality	r	RSR	NSE
Very good	> 0,9	< 0,5	> 0.7
Good	0,7 - 0,9	0,5 - 0,6	0.6 - 0.7
Satisfactory	0,5 - 0,7	0,6 - 0,7	0.5 - 0.6
Unsatisfactory	< 0,5	> 0,7	< 0.5

RMSE observed standard deviation ratio (RSR):

$$RSR = \sqrt{\frac{\sum_{i=1}^{n} (x_i - y_i)^2}{\sum_{i=1}^{n} (x_i - \overline{x_i})^2}} \tag{7}$$

The Root Mean Square Error to Standard Deviation Ratio (RSR) represents the ratio of the difference between two data series, namely model and observed data. A smaller RSR value indicates a higher degree of similarity between the two datasets. Additionally, the degree of agreement between the measured and calculated data is assessed using the Nash-Sutcliffe Efficiency (NSE) coefficient. The NSE coefficient is calculated using the following formula:

$$NSE = 1 - \frac{\sum_{i=n}^{1}\left(x_i - y_i\right)^2}{\sum_{i=n}^{1}\left(x_i - \bar{x}_i\right)^2} \quad (8)$$

In there: x_i: measured value at time i

y_i: calculated value at time i

$\bar{x}_i$: average measured value

The Nash-Sutcliffe coefficient (NSE) can range from - ∞ to 1. NSE=1 corresponds to a perfect match between the model and the observed data.

2.4.3. Calibration with the Doksuri storm in 2017

The calibration of results for the 2017 Doksuri storm was performed using two approaches: the reanalysis wind field method and a combined wind field method that integrates ERA5 reanalysis wind data with an experimental storm wind simulation, applied across the entire East Sea calculation domain, as depicted in Figure 2. The results were compared to ERA5 reanalysis wave data. The combined wind field method yielded higher values for the maximum wind radius, wind speed, and wave height in the storm-affected areas, particularly within the storm's eye region. Specifically, maximum wind speeds exceeded 26 m/s and maximum wave heights surpassed 6 m. Additionally, it was confirmed that the combined wind field method produced results more consistent with actual measurements, as shown in Figure 2e.

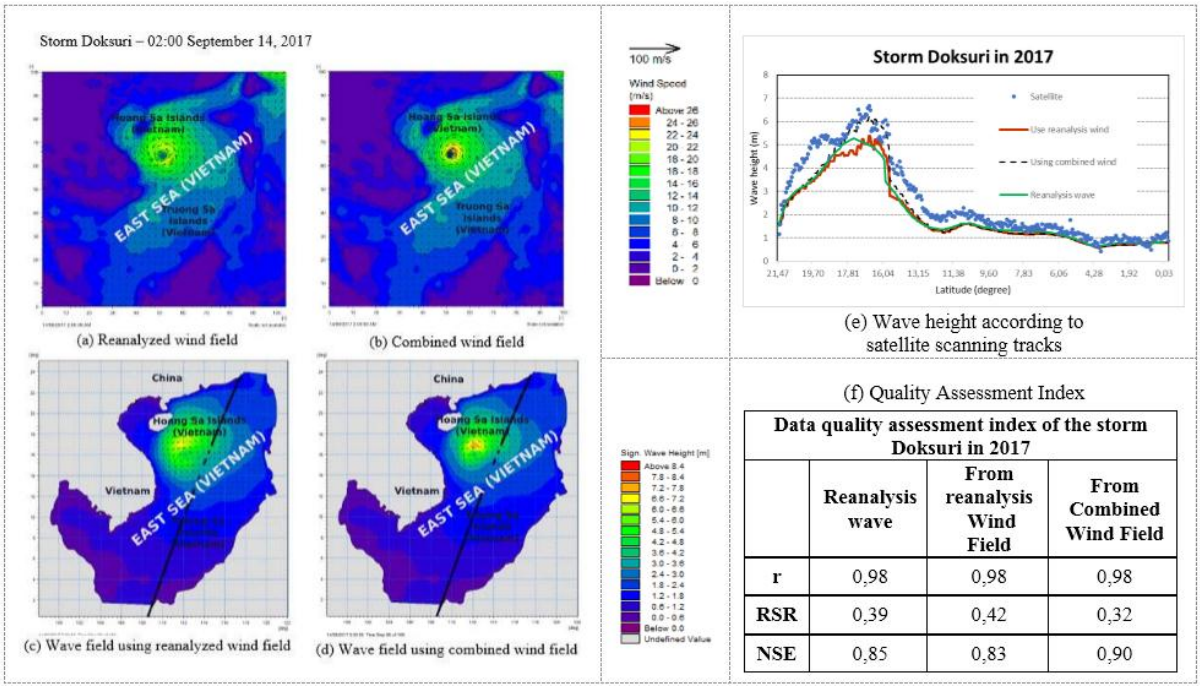

(a) Reanalyzed wind field

(b) Combined wind field

(c) Wave field using reanalyzed wind field

(d) Wave field using combined wind field

(e) Wave height according to satellite scanning tracks

(f) Quality Assessment Index

Data quality assessment index of the storm Doksuri in 2017			
	Reanalysis wave	**From reanalysis Wind Field**	**From Combined Wind Field**
r	0,98	0,98	0,98
RSR	0,39	0,42	0,32
NSE	0,85	0,83	0,90

Figure 2. Wind velocity field and wave height field in the East Sea during the Doksuri storm at 02:00 on September 14, 2017

Figure 2e illustrates the wave height based on satellite tracking during the Doksuri storm at 02:00 on September 14, 2017. In general, the wave heights are similar across all three scenarios for low to medium values. However, as wave heights reach extreme values during the storm, a noticeable discrepancy arises. The model scenario utilizing the reanalysis wind field, along with reanalysis wave data, produces lower values than the actual measurements at extreme time points. In contrast, when the combined wind field is used as input, the computed results align closely with the actual measurements and capture the extreme values, demonstrating superior accuracy compared to the scenarios relying solely on the reanalysis wind field or reanalysis wave data.

The model calibration results for the 2017 Doksuri storm, based on three statistical indices (r, RSR, and NSE) for two wind field input scenarios and a comparison with the quality of reanalysis wave data, are presented in Figure 2(f). According to the evaluation criteria outlined in Table 3, the quality of both the reanalysis wave data and the model calculations in both scenarios is classified as very good. The r index remains constant at 0.98, indicating a high correlation. Notably, the results from the combined wind field scenario surpass those from the reanalysis wind field scenario, as well as the reanalysis wave data, across the other two indices. The RSR index

for the reanalysis wind field scenario is 0.42, compared to 0.85 for the reanalysis wave data; however, when the combined wind field is used, the RSR improves to 0.32. A similar trend is observed for the NSE index, which initially stands at 0.83 for the reanalysis waves, and increases to 0.90 when the combined wind field is applied, both reflecting very good quality levels. Based on these evaluations, it can be concluded that following calibration with the Doksuri storm in 2017, the model using the combined wind field scenario yields results that are closer to actual measurements, with an acceptable margin of error.

III. Results and discussion

To assess the potential of combining reanalysis wind data with experimental storm wind data in storm wave simulations, the research team utilized the MIKE 21 SW model, which was calibrated for two calculation scenarios: 1) A scenario employing ERA5 reanalysis wind data as the input wind field, and 2) A scenario using a combined wind field that integrates ERA5 reanalysis wind data with wind data from the experimental storm wind model.

The set of three statistical indices used to evaluate the model's performance includes the Pearson correlation coefficient (r), the root mean square error (RMSE) ratio (RSR), and the Sutcliffe Nash efficiency coefficient (NSE). The quality assessment criteria for these indices are presented in Table 3.

Figure 3 presents the wave heights along the satellite tracks for seven selected storms. Blue circles represent satellite data, solid blue lines represent global ERA5 reanalysis wave data, solid red lines depict model results using the reanalysis wind field scenario, and dashed black lines show model results using the combined wind field scenario. In the reanalysis wind field scenario, the model results are lower than the measured data, with discrepancies increasing as wave heights rise. In contrast, the combined wind field scenario produces results that are more consistent and better capture the extreme values of the measured data. While some overestimations are observed in the Mawar 2017 case and certain extreme values are not captured in the Pabuk 2019, Etau 2020, and Lionrock 2021 cases, the improvement compared to the BD scenario is significant. Furthermore, a comparison with the reanalysis wave data shows that the combined wind field scenario provides better results, aligning more closely with the measured data and more effectively capturing the extreme values.

Evaluation of the simulation results quality according to the two wind field scenarios

Table 4 presents the evaluation results of the quality of two simulation methods based on two wind fields for seven selected storms, using three indices: r, RSR, and NSE. According to the evaluation criteria outlined in Table 3, the quality of both the reanalysis wave data and the model calculation results for both methods is classified as high.

1) Storm Sarika in 2016: Using the ERA5 wind field method, the correlation coefficient (r) between the calculated results and the measured data reached a very high level, comparable to the reanalysis wave data. After applying the combined wind field method, the calculated results showed further improvement, demonstrating better agreement with the measured data. Although the RSR index for the combined wind field method decreased relative to the ERA5 wind field method, it remained at a very good level. The NSE index for both the reanalysis wave data and the two model methods also achieved very high quality.

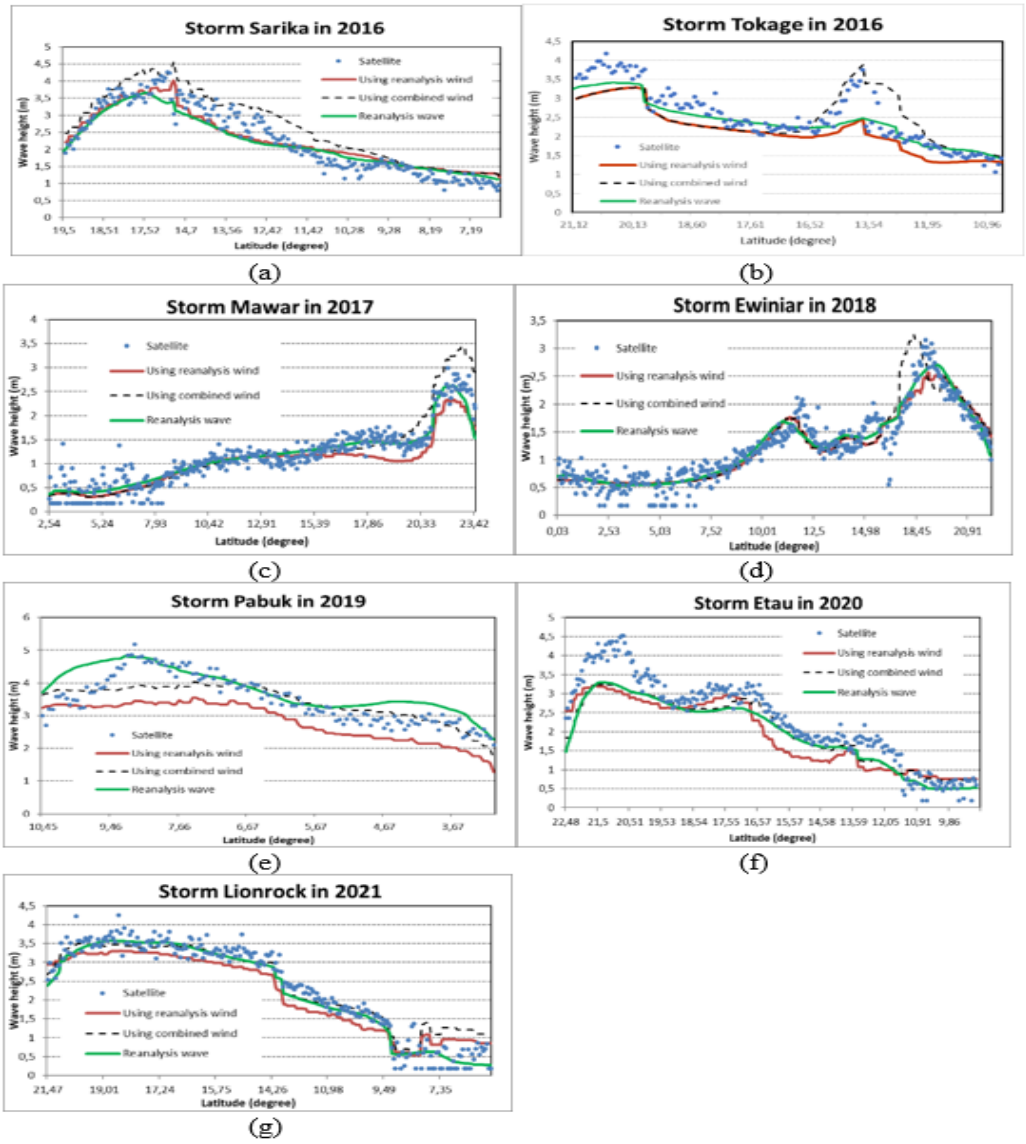

Figure 3. Wave height according to satellite track in 07 selected storms:

(a) Storm Sarika – 10:00 PM, October 16, 2016
(b) Storm Tokage – 11:00 AM, November 26, 2016
(c) Storm Mawar – 3:00 PM, September 3, 2017
(d) Storm Ewiniar – 7:00 AM, June 5, 2018
(e) Storm Pabuk – 11:00 PM, January 1, 2019
(f) Storm Etau – 04:00 AM, November 8, 2020
(g) Storm Lionrock – 08:00 AM, October 8, 2021

2) Storm Tokage in 2016: The r, RSR, and NSE indices indicate that while the quality of the model data using the combined wind field method decreased relative to the ERA5 wind field method and reanalysis wave data, it remained at a good and acceptable level.

3) Storm Mawar in 2017: The three indices (r, RSR, and NSE) demonstrate that the quality of the data in all three cases was very good. The correlation coefficient (r) was higher in the combined wind field method, while the RSR and NSE indices showed a slight decrease in quality for the combined wind field method compared to the ERA5 wind field method, though the results still maintained very good quality.

4) Storm Ewiniar in 2018: In all three cases, the indices were at very good levels. The results indicated that the data quality using the combined wind field method was superior to that of the ERA5 wind field method, with improvements observed across all three indices. All indices achieved very good quality, aligning with the evaluation standards for the reanalysis wave data.

Table 4. Evaluation indices of the quality of reanalysis wave data and model results according to two scenarios

	Reanalysis wave	From reanalysis Wind Field	From Combined Wind Field	Reanalysis wave	From reanalysis Wind Field	From Combined Wind Field
	Storm Sarika in 2016			**Storm Tokage in 2016**		
r	0,96	0,96	0,97	0,93	0,94	0,76
RSR	0,35	0,32	0,45	0,45	0,62	0,65
NSE	0,88	0,90	0,80	0,80	0,62	0,58
	Storm Mawar in 2017			**Storm Ewiniar in 2018**		
r	0,95	0,93	0,94	0,94	0,93	0,94
RSR	0,33	0,45	0,48	0,34	0,40	0,34
NSE	0,89	0,80	0,77	0,88	0,84	0,88
	Storm Pabuk in 2019			**Storm Etau in 2020**		
r	0,87	0,87	0,84	0,97	0,93	0,96
RSR	0,64	1,01	0,55	0,45	0,52	0,44
NSE	0,59	-0,01	0,7	0,80	0,73	0,81
	Storm Lionrock in 2021					
r	0,98	0,96	0,96			
RSR	0,21	0,32	0,3			
NSE	0,96	0,9	0,91			

5) Storm Pabuk in 2019: The indices indicate that the quality of the model data using the combined wind field method is significantly better than that of the ERA5 wind field method and reanalysis wave data, except for the correlation coefficient (r), which decreased but remained at a good level. Both the RSR and NSE indices improved from poor to good and very good, surpassing the quality of the reanalysis wave data.

6) Storm Etau in 2020: The indices in the combined wind field method showed significant improvement compared to the ERA5 wind field method and also outperformed the reanalysis wave data evaluation indices. The RSR index in the ERA5 wind field method was at a good level, whereas in the combined wind field method, it reached a very good level. Similarly, the NSE index improved, further demonstrating that the data quality from the combined wind field method was significantly superior to that of the ERA5 wind field method and also exceeded the quality of reanalysis wave data.

7) Storm Lionrock in 2021: The statistical indices for both the reanalysis wave data and the model results from both methods were at very good quality levels. The results indicate that the quality of the data from the combined wind field method improved compared to the ERA5 wind field method. Although the combined wind field method was slightly lower than the reanalysis wave data, the difference was minimal, as the r, RSR, and NSE indices all achieved very good levels.

General comments

The simulation results for seven storms from 2016 to 2021, using two input wind field scenarios, demonstrate that the wave height field in the combined wind field scenario is consistently higher than that in the ERA5 wind field scenario in areas affected by the storm winds. The most notable difference occurs at the storm's center, particularly when wave height reaches its peak. In the ERA5 wind field scenario, the model tends to underestimate the observed data at peak times. In contrast, the combined wind field scenario produces results that align more closely with the observed data and effectively capture extreme values. For the Mawar and Ewiniar storms, the model overestimated the observed data but still captured the extreme values. For the Pabuk, Etau, and Lionrock storms, although the model did not capture the peak values, the model-observed discrepancies were reduced. These findings highlight the advantage of combining two wind fields. Statistical indices indicate that the model quality in the combined wind field scenario is generally superior, except the Tokage storm, where the model quality decreased but remained acceptable. When compared to ERA5 reanalysis wave data across the storms, the model results from the combined wind field scenario were better at capturing extreme values and were closer to the observed data, while the ERA5 wind field scenario generally performed worse than the ERA5 reanalysis wave data.

IV. Conclusion and recommendations

This study utilizes the MIKE 21 SW model to simulate the extreme wave field in the East Sea (Vietnam) under two scenarios: one incorporating reanalysis wind fields and the other utilizing combined wind fields, which consist of ERA5 reanalysis wind data and storm wind data from an experimental model. The model was calibrated using the 2017 Doksuri storm and subsequently applied to simulate the wave field during seven storms over six years, from 2016 to 2021.

The simulation results for the storms under both scenarios indicate that, with the combined wind field, wave heights in areas affected by the storm are higher compared to the ERA5 wind field scenario, particularly near the storm's center, where the difference is most pronounced as wave heights reach their peak values. The wave field derived from the ERA5 wind field tends to underestimate the observed data at peak times. In contrast, the combined wind field scenario results in wave height data that are more closely aligned with observed values and effectively capture the extreme values. Specifically, for the Mawar and Ewiniar storms, the model results overestimated the observed values but still captured the extreme values. For the Pabuk, Etau, and Lionrock storms, while the model did not capture the extreme values, the discrepancies between the model and observed data were significantly reduced. Statistical indices further demonstrate an improvement in model performance using the combined wind field, except in the case of Storm Tokage, where model quality slightly decreased but remained within an acceptable range. Compared to ERA5 reanalysis wave data, the model results using the combined wind field scenario better capture the extreme values and are closer to the observed data, while the ERA5 wind field model generally performs worse.

Therefore, it can be concluded that using the combined wind field model results in simulations that are more aligned with observed data, both qualitatively and quantitatively, with acceptable error margins.

The results of this study are significant as it represents the first research to use a combined wind field, comprising ERA5 reanalysis wind and experimental storm wind data, as inputs for simulating the wave field during storms in the East Sea (Vietnam). This approach addresses the issue of wave height underestimation during extreme wave events, which is common in global reanalysis wave datasets and many previous studies. The high-quality simulations of extreme waves provide valuable data that supplement the scarcity of extreme wave data, thereby enhancing the quality of synthesized wave data for the East Sea (Vietnam).

A limitation of this study is its exclusive focus on wave height. To further enhance the quality of wave field simulations during storms, future research should incorporate additional parameters, such as wave direction and wave period, for each storm. The next step for the research team will be to address this limitation while also conducting new studies to complete the reanalyzed wave dataset for the East Sea (Vietnam) region.

Author Contributions: Research idea generation- methodology, N.X.H., D.N.T., N.T.T.; Data processing, N.T.T, C.H.A., P.V.C.; writing—original draft preparation, D.N.T.,V.T.V., C.H.A, P.V.C.; writing—review and editing, N.X.H., D.N.T., V.T.V. All authors have read and agreed to the published version of the manuscript.

Fundings: The article was completed with the support of the Ministry of Natural Resources and Environment project “Research on building a wave field reanalysis data system based on numerical models, assimilation techniques and observation data for forecasting and warning of ocean waves in Vietnam's sea areas”, code TNMT.2023.06.13.

Data Availability Statement: Data are contained within the article.

Conflicts of Interest: The authors declare that this article is their own research work, has not been previously published, is not copied or plagiarized; there is no conflict of interest among the authors.

References

[1]. Cavaleri, L.; Alves, J.; Ardhuin, F.; Babanin, A.; Banner, M.; Belibassakis, K.; Benoit, M.; Donelan, M.; Groeneweg, J.; Herbers, T.; Hwang, P.; Janssen, P.A.E.M.; Janssen, T.; Lavrenov, I.V.; Magne, R.; Monbaliu, J.; Onorato, M.; Polnikov, V.; Resio, D.; Rogers, W.E.; Sheremet, A.; McKee Smith, J.; Tolman, H.L.; van Vledder, G.; Wolf, J.; Young, I. Wave modelling: The state of the art. Prog. Oceanogr. **2007**, 75(4), 603–674.

[2]. Akpinar, A.; van Vledder, G.P.; Kömürcü, M.I.; Özger, M. Evaluation of the numerical wave model (SWAN) for wave simulation in the Black Sea. Cont. Shelf Res. **2012**, 50–51, 80–99.

[3]. Cavaleri, L.; Sclavo, M. The calibration of wind and wave model data in the Mediterranean sea. Coastal Eng. **2006**, 53, 613–627.

[4]. Booij, N.; Ris, R.; Holthuijsen, L. A third generation wave model for coastal region, I: Model description and validation. J. Geophys. Res. **1999**, 104, 769–7666.

[5]. Cox, A.; Swail, V. A global wave hindcast over the period 1958–1997: Validation and climate assessment. J. Geophys. Res. **2001**, 106, 2313–2329.

[6]. Dodet, G.; Bertin, X.; Taborda, R. Wave climate variability in the north-east Atlantic Ocean over the last six decades. Ocean Model. **2010**, 31, 120–131.

[7]. Tolman, H.L.; Balasubramaniyan, B.; Burroughs, L.D.; Chalikov, D.V.; Chao, Y.Y.; Chen, H.S.; Gerald, V.M. Development and implementation of wind-generated ocean surface wave models at NCEP. Weather Forecast. **2002**, 17(2), 311–333.

[8]. Nguyen, H.; Duong, T.; Nguyen, T.; Pham, C. Study on adjustment of wave reanalysis data from global models for the coastal area of Central Vietnam (in Vietnamese). Journal of Climate Change Science. **2024**, 29, 77–84.

[9]. Nguyen, H.; Duong, T.; Vu, V.; Giap, A.; Cao, A. Evaluate the applicability of reanalyzed wave data for the East Sea (in Vietnamese). Vietnam Journal of Hydrometeorology. **2025**, 769, 14–26.

[10]. Chen, W.B.; Lin, L.Y.; Jang, J.H.; Chang, C.H. Simulation of typhoon-induced storm tides and wind waves for the northeastern coast of Taiwan using a tide-surge-wave coupled model. Water **2017**, 9, 549.
[11]. Marsooli, R.; Lin, N. Numerical modeling of historical storm tides and waves and their interactions along the U.S. East and Gulf Coasts. J. Geophys. Res.: Oceans **2018**, DOI: 10.1002/2017JC013434.
[12]. Tolman, H.L.; Balasubramaniyan, B.; Burroughs, L.D.; Chalikov, D.V.; Chao, Y.Y.; Chen, H.S.; Gerald, V.M. Development and implementation of wind-generated ocean surface wave models at NCEP. Weather Forecast. **2002**, 17, 311–333.
[13]. Xu, F.; Perrie, W.; Toulany, B.; Smith, P.C. Wind-generated waves in Hurricane Juan. Ocean Model. **2007**, 16, 188–205.
[14]. Young, I.R. Directional spectra of hurricane wind waves. J. Geophys. Res.: Oceans **2006**, 111. C08020, doi:10.1029/2006JC003540.
[15]. Hoque, M.A.; Perrie, W.; Solomon, S.M. Application of SWAN model for storm-generated wave simulation in the Canadian Beaufort Sea. J. Ocean Eng. Sci. **2020**, 5, 19–34.
[16]. Rusu, L.; Bernardino, M. Influence of the wind fields on the accuracy of numerical wave modelling in offshore locations. J. Ocean Eng. **2008**.
[17]. Van Vledder, G.P.; Akpinar, A. Wave model predictions in the Black Sea: Sensitivity to wind fields. Appl. Ocean Res. **2015**, 53, 161–178.
[18]. Campos, R.M.; Alves, J.H.G.M.; Guedes Soares, C.; Guimaraes, L.G.; Parente, C.E. Extreme wind-wave modeling and analysis in the South Atlantic Ocean. Ocean Model. **2018**, 124, 75–93.
[19]. Hersbach, H.; Bell, B.; Berrisford, P.; Hirahara, S.; Horányi, A.; Muñoz-Sabater, J.; Nicolas, J.; Peubey, C.; Radu, R.; Schepers, D.; Simmons, A.; Soci, C.; Abdalla, S.; Abellan, X.; Balsamo, G.; Bechtold, P.; Biavati, G.; Bidlot, J.; Bonavita, M.; De Chiara, G.; Dahlgren, P.; Dee, D.; Diamantakis, M.; Dragani, R.; Flemming, J.; Forbes, R.; Fuentes, M.; Geer, A.; Haimberger, L.; Healy, S.; Hogan, R.J.; Hólm, E.; Janisková, M.; Keeley, S.; Laloyaux, P.; Lopez, P.; Lupu, C.; Radnoti, G.; de Rosnay, P.; Rozum, I.; Vamborg, F.; Villaume, S.; Thépaut, J.N. The ERA5 global reanalysis. Q. J. R. Meteorol. Soc. **2020**, 146, 1999–2049.
[20]. Wiese, A.; Staneva, J.; Schulz-Stellenfleth, J.; Behrens, A.; Fenoglio-Marc, L.; Bidlot, J.R. Synergy of wind wave model simulations and satellite observations during extreme events. Ocean Sci. **2018**, 14, 1503–1521.
[21]. Powell, M.D.; Murillo, S.; Dodge, P.; Uhlhorn, E.; Gamache, J.; Cardone, V.; Cox, A.; Otero, S.; Carrasco, N.; Annane, B.; Fleur, R.S. Reconstruction of Hurricane Katrina's wind fields for storm surge and wave hindcasting. Ocean Eng. **2010**, 37, 26–36.
[22]. Sheng, Y.P.; Zhang, Y.; Paramygin, V.A. Simulation of storm surge, wave, and coastal inundation in the Northeastern Gulf of Mexico region during Hurricane Ivan in 2004. Ocean Model. **2010**, 35, 314–331.
[23]. Willoughby, H.E.; Darling, R.W.R.; Rahn, M.E. Parametric representation of the primary hurricane vortex. Part II: A new family of sectionally continuous profiles. Mon. Weather Rev. **2006**, 134, 1102–1120.
[24]. Tolman, H.L.; Alves, J.H.G.M. Numerical modeling of wind waves generated by tropical cyclones using moving grids. Ocean Model. **2005**, 9, 305–323.
[25]. Boose, E.; Foster, D.; Fluet, M. Hurricane impacts to tropical and temperate forest landscape. Ecological Monographs. **1994**, 64(4), 369-400.
[26]. Website: https://cds.climate.copernicus.eu/datasets/reanalysis-era5-single-levels?tab=download
[27]. Website: http://agora.ex.nii.ac.jp/digital-storm/index.html.en
[28]. Pham, N.; Le, H.; Pham, T.; Doan, H.; Tran, T.; Nguyen, A.; Bui, H. Wave analysis for the development of Thien Nga - Hai Au oil field. Journal of Climate Change Science. **2023**, 27, 11–22.